BBS7 is required for BBSome formation and its absence in mice results in Bardet-Biedl syndrome phenotypes and selective abnormalities in membrane protein trafficking

Qihong Zhang[1], Darryl Nishimura[1], Tim Vogel[2], Jianqiang Shao[3], Ruth Swiderski[1], Terry Yin[4], Charles Searby[1], Calvin S. Carter[5], GunHee Kim[1], Kevin Bugge[1], Edwin M. Stone[6] and Val C. Sheffield[1,*]

[1]Department of Pediatrics, Howard Hughes Medical Institute, University of Iowa, Iowa City, IA 52242, USA
[2]Department of Neurosurgery, University of Iowa, Iowa City, IA 52242, USA
[3]Central Microscopy Research Facilities, University of Iowa, Iowa City, IA 52242, USA
[4]Department of Internal Medicine, University of Iowa, Iowa City, IA 52242, USA
[5]Program in Neuroscience, University of Iowa, Iowa City, IA 52242, USA
[6]Department of Ophthalmology and Visual Sciences, Howard Hughes Medical Institute, University of Iowa, Iowa City 52242, USA
*Author for correspondence (val-sheffield@uiowa.edu)

Accepted 18 March 2013
Journal of Cell Science 126, 2372–2380

doi: 10.1242/jcs.111740

Summary

Bardet-Biedl Syndrome (BBS) is a pleiotropic and genetically heterozygous disorder caused independently by numerous genes (*BBS1–BBS17*). Seven highly conserved BBS proteins (BBS1, 2, 4, 5, 7, 8 and 9) form a complex known as the BBSome, which functions in ciliary membrane biogenesis. BBS7 is both a unique subunit of the BBSome and displays direct physical interaction with a second BBS complex, the BBS chaperonin complex. To examine the *in vivo* function of BBS7, we generated *Bbs7* knockout mice. *Bbs7*$^{-/-}$ mice show similar phenotypes to other BBS gene mutant mice including retinal degeneration, obesity, ventriculomegaly and male infertility characterized by abnormal spermatozoa flagellar axonemes. Using tissues from *Bbs7*$^{-/-}$ mice, we show that BBS7 is required for BBSome formation, and that BBS7 and BBS2 depend on each other for protein stability. Although the BBSome serves as a coat complex for ciliary membrane proteins, BBS7 is not required for the localization of ciliary membrane proteins polycystin-1, polycystin-2, or bitter taste receptors, but absence of BBS7 leads to abnormal accumulation of the dopamine D1 receptor to the ciliary membrane, indicating that BBS7 is involved in specific membrane protein localization to cilia.

Key words: BBSome, Bardet Biedl syndrome, Cilia, Protein trafficking

Introduction

Cilia are microtubule-based structures that extend from the cell surface of most eukaryotic cells. They contain unique cell membrane components separate from the plasma membrane and are classified as either motile or primary cilia (immotile). Cilia play an important role during development and in adult tissue physiology. Cilia defects lead to a wide range of human diseases termed ciliopathies that include primary ciliary dyskinesis, polycystic kidney disease, nephronophthisis, Joubert syndome, Senior-Loken syndrome, Meckel-Gruber syndrome, oro-facial-digital syndrome, Alstrom syndrome, and Bardet-Biedl syndrome (BBS).

BBS is an autosomal recessive genetic disorder characterized by obesity, retinopathy, polydactyly, renal malformations, learning disabilities and hypogenitalism as well as secondary defects including diabetes and hypertension. To date, 17 BBS genes are reported to independently cause the disorder (Sattar and Gleeson, 2011). Although the cellular functions of BBS proteins are not yet fully understood, functional studies in model organisms have revealed that BBS proteins are involved in ciliary functions and intracellular transport. In *Caenorhabditis elegans*, bbs genes are expressed in ciliated neurons and localize to the ciliary base/transition zone and participate in IFT along the ciliary axoneme. *bbs7* and *bbs8* mutant *C. elegans* lines have dye filling defects, shorter cilia, and defects in intraflagellar transport (IFT) (Blacque et al., 2004). Knockdown of expression of *bbs* genes in zebrafish results in Kupffer's vesicle defects, premature cilia loss, and retrograde melanosome transport delay (Yen et al., 2006). BBS mutant mice recapitulate the retinal degeneration and obesity phenotypes seen in BBS patients. In addition, male BBS mutant mice lack spermatozoa flagella (Davis et al., 2007; Fath et al., 2005; Mykytyn et al., 2004; Nishimura et al., 2004). Biochemical studies show that seven of the known BBS proteins (BBS1, 2, 4, 5, 7, 8, and 9) form a stable complex known as the BBSome (Nachury et al., 2007). Other BBS proteins including BBS6, BBS10, and BBS12 form a complex that regulates BBSome assembly (Seo et al., 2010). One of the functions of the BBSome is to promote cilia membrane biogenesis through the small GTPase Rab8 and serves as coat complex for ciliary membrane protein trafficking (Jin et al., 2010; Nachury et al., 2007).

Although BBS mutant mice recapitulate most of the BBS phenotypes, phenotypic differences are observed among different

BBS gene mutations. For example, *Bbs4*$^{-/-}$ and *Bbs6*$^{-/-}$ mice are hypertensive, while *Bbs2*$^{-/-}$ mice are normotensive (Rahmouni et al., 2008). *Bbs3*$^{-/-}$ mice have more severe hydocephalus and are less obese than other BBS mice (Zhang et al., 2011). Consistent with mouse studies, BBS patients display phenotypic variability both between and within families. Physiological differences among BBS patients caused by mutations in distinct genes have been documented (Feuillan et al., 2011; Kulaga et al., 2004), suggesting that although sharing common BBS phenotypes, different BBS genes may possess unique functions. BBS7 is unique in that it is a subunit of the BBSome and directly interacts physically with the BBS chaperonin complex. In order to study the role of BBS7 *in vivo* and to determine if loss of *Bbs7* has any associated unique phenotypes, we generated *Bbs7* knockout mice. *Bbs7*$^{-/-}$ mice show similar phenotypes to those observed in other BBS mutant mice including retinal degeneration, lack of spermatozoa flagella, obesity, and ventriculomegaly. We demonstrate that BBS7 and BBS2 depend on each other for protein stability and that BBS7 is required for BBSome formation. Notably, we show that the BBSome is not required for universal ciliary membrane protein localization; however, absence of BBS7 leads to abnormal accumulation of D1R to the ciliary membrane.

Results

Generation of *Bbs7* null mice

BBS7 is unique among BBS proteins in that it is an integral part of the BBSome and a component of the BBS chaperonin complex. To investigate the *in vivo* function of the *Bbs7* gene, we generated *Bbs7* gene knockout mice by replacing exon 5 with a neomycin cassette. This causes a frameshift resulting in a null *Bbs7* allele (supplementary material Fig. S1A). The absence of *Bbs7* mRNA was verified by RT-PCR analysis using RNA isolated from *Bbs7*$^{-/-}$ mouse testes with primers within exon 5 (supplementary material Fig. S1B). The absence of BBS7 protein was confirmed by western blotting (supplementary material Fig. S1C).

Mating of *Bbs7*$^{+/-}$ heterozygotes resulted in 26% *Bbs7*$^{+/+}$ mice, 55% *Bbs7*$^{+/-}$ mice, and 19% *Bbs7*$^{-/-}$ mice (n=387; P<0.05). The decreased frequency of *Bbs7*$^{-/-}$ offspring has been observed in other BBS mutant mice and suggests that some of the *Bbs7*$^{-/-}$ mice died prenatally or perinatally.

Bbs7$^{-/-}$ mice become obese, lack kidney cysts and do not develop polydactyly

Bbs7$^{-/-}$ mice are runts at birth, weigh less than their littermates at 3 weeks of age, and become obese over time. After weaning, *Bbs7*$^{-/-}$ mice begin to gain more weight than wild-type mice due to increased food intake. By 12 weeks of age, *Bbs7*$^{-/-}$ mice (both male and female) weigh significantly more than their control littermates, and the differences become greater in older animals. By 7 months, wild-type mice are 28.7±2.8 g versus *Bbs7*$^{-/-}$ 41.1±3.25 g (P<0.05).

Although renal abnormality and polydactyly are cardinal features of the BBS phenotypes in humans, we did not observe renal cysts or polydactyly of the forelimbs or hindlimbs in the *Bbs7* mutant mice, suggesting species difference or threshold differences between mouse and human.

Bbs7$^{-/-}$ mice exhibit retinal degeneration and ventriculomegaly

Histological analysis of 4–8-month-old *Bbs7*$^{-/-}$ eyes demonstrated a significant degeneration of the inner and outer segments of the photoreceptor cells and of the outer nuclear layer (Fig. 1A,B). Ventriculomegaly was observed in the lateral and third ventricles of the brain as seen in coronal sections of 4–8-month-old *Bbs7*$^{-/-}$ mice (Fig. 1C–F). We also observed thinning of the cerebral cortex and a reduction in the size of the hippocampus and corpus striatum. No gross abnormalities in the cerebellum were observed in the *Bbs7* mutant mice or other BBS mutant mice (supplementary material Fig. S2).

Bbs7$^{-/-}$ mice have abnormal motile cilia in the brain ependymal layer

Since BBS is a cilia-related disease, we examined motile cilia and primary cilia in the *Bbs7*$^{-/-}$ mice. We examined the motile cilia of the ependymal cell layer lining the ventricles by staining coronal sections of 3-month-old wild-type and *Bbs7*$^{-/-}$ mouse brains with an anti-acetylated α-tubulin antibody and anti-IFT88 antibody as cilia markers. Compared to controls, *Bbs7*$^{-/-}$ mice show a greatly reduced number of ependymal cell cilia and the remaining cilia are shorter (Fig. 2A,B).

To further analyze the motile cilia in the brain ependymal layer, we performed TEM analysis of 3-week-old wild-type and *Bbs7*$^{-/-}$ mice brains. The motile cilia from *Bbs7*$^{-/-}$ brain ependymal layer have short, bulged cilia with vesicles (Fig. 2C,D) and those motile cilia also have defective axonemal structures (Fig. 2F,G) compared to wild-type controls

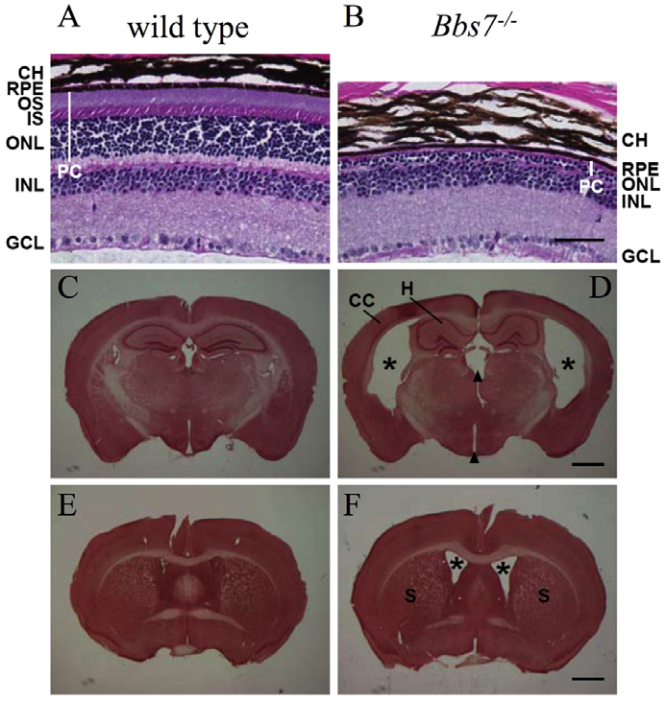

Fig. 1. *Bbs7*$^{-/-}$ mice display photoreceptor cell loss and ventriculomegaly. (**A**,**B**) H&E-stained 4–8-month-old wild-type (A) and *Bbs7*$^{-/-}$ (B) eyes show loss of photoreceptor inner and outer segments as well as degeneration of the outer nuclear layer. PC, photoreceptor cells. (**C–F**) Neutral-Red-stained 60–100 μm-thick coronal brain sections from wild-type (C,E) and *Bbs7*$^{-/-}$ mice (D,F) show enlarged lateral ventricles (*), an enlarged dorsal third ventricle (upper and lower arrowhead), reduced corpus striatum (S) and hippocampus (H), and thinning of the cerebral cortex (CC). Scale bars: 50 μm (A,B); 1 mm (C–F).

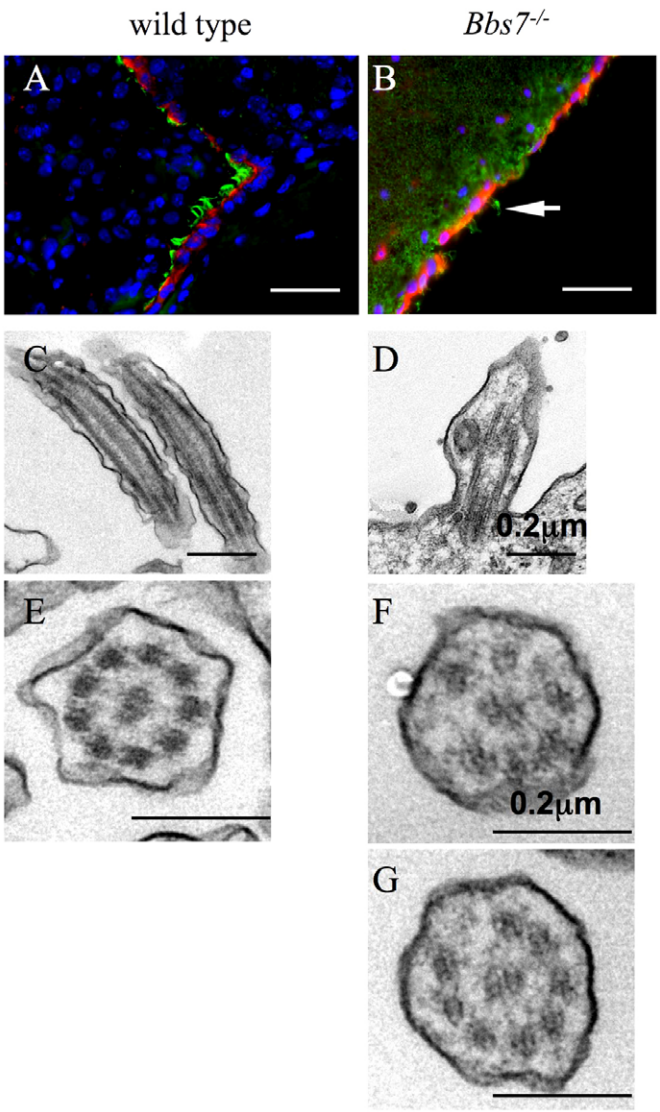

Fig. 2. *Bbs7*$^{-/-}$ mice have abnormal motile cilia in the brain ependymal layer. (**A**,**B**) Immunofluorescent staining of brain ventricle ependymal cells using anti-acetylated α-tubulin (green) and anti-IFT88 antibody (red) revealed the lack of cilia and short cilia (arrow) in the ependymal layer of *Bbs7*$^{-/-}$ mice (A) compared with wild-type controls (B). (**C**,**D**) TEM analysis of longitudinal section of motile cilia in the brain ependymal layer shows short and bulged cilia with vesicles in 3-week-old *Bbs7*$^{-/-}$ mice (D) compared with 3-week-old wild-type control (C). (**E–G**) TEM analysis of cross-section of motile cilia in the brain ependymal layer shows abnormal axonemal structure in *Bbs7*$^{-/-}$ mice (F,G) compared with wild-type control (E). Scale bars: 50 μm (A,B); 0.2 μm (C–G).

(Fig. 2E). These studies indicate that the absence of BBS7 protein affects motile cilia structures.

To examine the primary cilia *in vivo*, we stained tissue sections from the kidney and the pancreas with acetylated α-tubulin. We did not find differences in primary cilia numbers or cilia length between wild-type and *Bbs7*$^{-/-}$ mice (supplementary material Fig. S3). Primary cilia also formed and appear normal in cultured kidney epithelial cells and cultured embryonic fibroblasts (MEF) derived from *Bbs7*$^{-/-}$ mice (supplementary material Fig. S3 and data not shown), although we cannot rule out the possibility that they may have subtle structural defects, such as post-modification changes in microtubules.

Bbs7$^{-/-}$ mice have abnormal sperm flagella

We previously demonstrated the absence of sperm flagella in *Bbs1*$^{M390R/M390R}$ knockin, *Bbs2*$^{-/-}$, *Bbs4*$^{-/-}$ and *Bbs6*$^{-/-}$ mice (Davis et al., 2007; Fath et al., 2005; Mykytyn et al., 2004; Nishimura et al., 2004). Hematoxylin and eosin staining of 4–8-month-old *Bbs7*$^{-/-}$ testes revealed a paucity of sperm flagella (Fig. 3A,B). We further refined this observation by immunofluorescence staining of testes tissue. While most

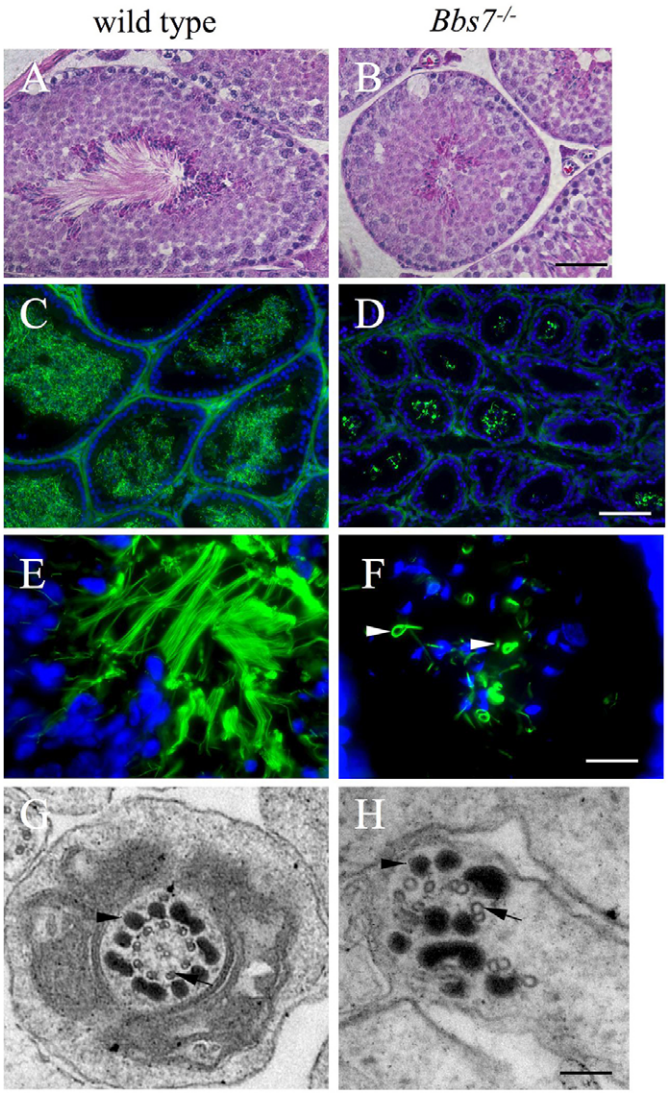

Fig. 3. *Bbs7*$^{-/-}$ mice have abnormal sperm flagella. (**A**,**B**) H&E stained 4–8-month-old wild-type (A) and *Bbs7*$^{-/-}$ (B) seminiferous tubules show a lack of spermatozoa flagella. (**C–F**) Immunofluorescent staining of testes flagella using anti-acetylated α-tubulin staining showed defects in *Bbs7*$^{-/-}$ mice. A ring-type of microtubule structure was frequently observed in *Bbs7*$^{-/-}$ mice. C and D are low power images, E and F are high power images. (**G**,**H**) TEM analysis of cross-section of wild-type (G) and *Bbs7*$^{-/-}$ (H) sperm flagella reveals that *Bbs7*$^{-/-}$ sperm flagella do not have typical 9+2 axonemes, but exhibit disorganized microtubule structures (arrow) and outer dense fibers (arrow head) surrounding the microtubular structures. Scale bars: 100 μm (A,B); 50 μm (C,D); 20 μm (E,F); 0.1 μm (G,H).

sperm from *Bbs7*$^{-/-}$ mice lack a flagellar tail, some of the sperm have malformed flagella. These abnormal flagella frequently form a ring type structure (Fig. 3C–F). To examine these malformed flagella in more detail, sections of wild-type and *Bbs7*$^{-/-}$ testes were analyzed by transmission electron microscopy (TEM). The microtubular structures and the outer dense fibers surrounding the microtubular structure in the principal piece are highly disorganized in the mutants (Fig. 3G,H). Occasionally we observed normal 9+2 axonemal structures in *Bbs7*$^{-/-}$ mice (8.8% vs 100% in wild-type, $P<0.01$). In contrast, the axonemal structures of motile cilia in the trachea of *Bbs7*$^{-/-}$ mice are largely normal by TEM analysis (supplementary material Fig. S4).

BBS7 is required for the BBSome formation

Since *Bbs7*$^{-/-}$ mice have similar phenotypes as other BBSome subunit knockout mice and BBS7 is a subunit of the BBSome, we investigated the effects of its loss on BBSome formation. Surprisingly, BBS2 protein levels were significantly decreased in *Bbs7*$^{-/-}$ testes protein lysates, but not in *Bbs4*$^{-/-}$ testes. Similarly, BBS7 protein levels were decreased in *Bbs2*$^{-/-}$ testes, but not in *Bbs4*$^{-/-}$ testes (Fig. 4A). To determine whether this was due to protein degradation or decreased transcription, we used semi-quantitative RT-PCR to evaluate *Bbs2* and *Bbs7* mRNA expression levels. We did not observe expression differences of *Bbs2* mRNA in *Bbs7*$^{-/-}$ testes or *Bbs7* mRNA differences in *Bbs2*$^{-/-}$ testes compared to controls (Fig. 4B). Together these results indicate that BBS2 and BBS7 protein level differences result from differences in protein stability, and that BBS2 and BBS7 are dependent on each other for stability.

The interdependence of BBS2 and BBS7 for protein stability is consistent with results showing that BBS2 physically interacts with BBS7 and forms a subcomplex (Nachury et al., 2007). Interestingly, BBS7 and BBS2 share coiled-coil domain sequence homology in their central regions (supplementary material Fig. S5). The BBS7 coiled-coil domain is not required for binding to BBS2. Instead, the C-terminal 200 amino acids of BBS7 are required for binding to BBS2 (supplementary material Fig. S5A). Similarly, the coiled-coil domain of BBS2 is not absolutely required for the interaction with BBS7, but loss of this domain decreases the interaction with BBS7 (supplementary material Fig. S5B). Furthermore, deletion of the coiled-coil region in BBS7 did

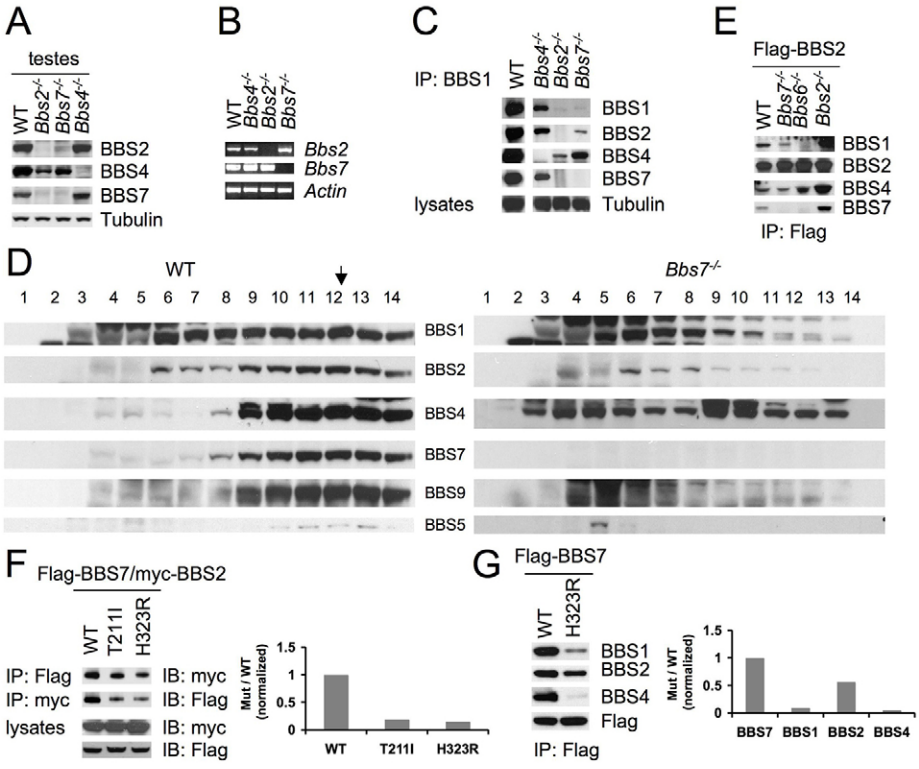

Fig. 4. BBS7 is required for BBSome formation. (**A**) BBS7 and BBS2 depend on each other for protein stability. Shown are western blots of total protein lysates from wild-type (WT), *Bbs2*$^{-/-}$, *Bbs4*$^{-/-}$ and *Bbs7*$^{-/-}$ testes. (**B**) RT-PCR analysis shows no apparent changes in *Bbs2* mRNA levels in *Bbs7*$^{-/-}$ mice nor changes in *Bbs7* mRNA levels in *Bbs2*$^{-/-}$ mice. (**C**) The BBSome does not form in BBS knockout mouse testes. Shown are western blots of testes proteins immunoprecipitated by anti-BBS1 antibody. The existence of other BBSome subunits was detected with antibodies against individual BBSome subunits. Equal amounts of initial protein from testes lystaes were used for immunoprecipitation. (**D**) Sucrose gradient analysis of testes protein lysates demonstrate that no BBSome forms in the absence of BBS7. (**E**) Loss of BBSome formation in cultured kidney cells from BBS knockout mice and BBS2 rescued BBSome formation in *Bbs2*$^{-/-}$ kidney cells. Shown are cultured kidney cells from different BBS knockout mice infected with adenovirus expressing FLAG-BBS2. Infected cells were lysed and expressed proteins were pulled down by anti-FLAG antibody. The existence of endogenous BBSome subunits was detected by western blot. (**F**) FLAG-BBS7 (WT and mutants) were co-transfected with myc-tagged BBS2 into 293T cells and the interaction between BBS7 and BBS2 was assayed by co-immunoprecipitation and quantified by ImageJ. (**G**) FLAG-BBS7 (WT and H323R mutation) were transfected into 293T cells and transfected proteins were pulled down by an anti-FLAG antibody. The presence of endogenous BBSome subunits was determined by anti-BBS1, BBS2, BBS4 and BBS7 antibodies. The amounts of BBS1, BBS2, BBS4 and BBS7 were quantified by ImageJ.

not disrupt its interaction with other endogenous BBSome subunits. BBS2 protein with deletion of the coiled-coil region disrupts the interaction with some of the endogenous BBSome subunits (BBS7) while maintaining the ability to interact with other BBSome subunits (BBS1 and BBS9) (supplementary material Fig. S5C).

To examine BBSome formation in the absence of BBS7, we performed immunoprecipitation with an antibody against BBS1, one of the subunits of the BBSome. The presence of other BBSome subunits in BBS1 pull-downs was decreased or undetectable in the absence of BBS7 or BBS2 as demonstrated by western blot. This indicates that the intact BBSome is not formed in the absence of BBS7 (Fig. 4C). We further confirmed these results by sucrose gradient analysis of total protein lysates from wild-type and *Bbs7*$^{-/-}$ testes (Fig. 4D).

To investigate whether the requirement of BBS7 for BBSome formation is unique to testes tissue, we isolated kidney primary epithelial cells from both wild-type and *Bbs7*$^{-/-}$ mice and infected the cultured cells with adenovirus expressing FLAG-BBS2. We pulled down FLAG-BBS2 and detected the existence of endogenous BBSome subunits using anti-BBS antibodies (Fig. 4E). We found that in the absence of BBS7 protein, no complete BBSome (minus BBS7) is formed, although some of the BBSome components still form a subcomplex. Whether these subcomplexes retain some residual functions is a question of interest.

To evaluate the impact on BBSome formation of homozygous BBS7 missense mutations (T211I and H323R) found in BBS patients, we tested whether BBS7 containing these mutations can be incorporated into the BBSome. Phylogenetic analysis shows that these mutations are located in conserved regions of the protein. We generated the mutated BBS7 constructs by site-directed mutagenesis and tagged them with FLAG at the N-terminus of the proteins. Mutated BBS7 proteins have decreased ability to interact with BBS2 as demonstrated by co-immunoprecipitation when co-transfected into 293T cells (Fig. 4F). The BBS7 H323R missense mutation has decreased ability to pull down endogenous BBSome subunits compared to wild-type BBS7 protein (Fig. 4G). A similar result was obtained with the T211I mutant protein (Zhang et al., 2012b). These results indicate that the BBS7 missense mutations affect BBSome formation. This provides an explanation as to why these homozygous point mutations cause BBS. In contrast, absence of BBS7 did not affect protein levels of IFT complex components or IFT complex formation (supplementary material Fig. S6A,B). Loss of BBS7 did not affect IFT protein ciliary localization (supplementary material Fig. S6C), consistent with the facts that loss of BBS genes has milder phenotypes than that of loss of IFT genes, although we do not know if the rate of IFT movement is altered.

BBS7 is not required for ciliary localization of taste receptors, polycystin-1 or polycystin-2

It is known that the BBSome is involved in cilia membrane biogenesis through Rab8. In addition, knock down of *bbs* genes in zebrafish results in defects in Kuffer's vesicle and retrograde melanosome transport delay. Furthermore, loss of BBS proteins results in accumulation of the sonic hedgehog pathway component Smoothened (Smo) inside cilia without pathway activation (Zhang et al., 2012a). These studies imply that BBS proteins function in specific vesicle trafficking. It has been shown that other cilia related proteins such as AHI1 and FUZZY are involved in general membrane protein trafficking rather than solely for cilia membrane protein trafficking (Gray et al., 2009; Hsiao et al., 2009). To test whether BBS7 is involved in general membrane protein trafficking, we examined clathrin-independent and clathrin-dependent endocytosis pathways in cultured wild-type and *Bbs7*$^{-/-}$ kidney primary cells using fluorophore labeled cholera toxin and transferrin receptor as markers, respectively. No differences of cholera toxin or transferrin receptor endocytosis were detected between wild-type and *Bbs7*$^{-/-}$ cells (supplementary material Figs S7, S8). Similar results are obtained using MEF cells from wild-type and *Bbs7*$^{-/-}$ mice. These data indicate that Bbs7 is not involved in general vesicular trafficking, but rather participates in specific types of vesicular trafficking such as melanosome transport in zebrafish and/or trafficking to specific subcellular destinations such as ciliary membranes.

Next, we examined ciliary membrane protein trafficking in Bbs7 null cells. Bitter taste receptors have recently been shown to localize to the ciliary membrane in the motile cilia of airway epithelium and taste receptor polymorphisms are associated with respiratory infection (Lee et al., 2012; Shah et al., 2009). Although there is no apparent phenotype in the kidney, an association of the bitter taste receptor with a specific type of nephropathy, Balkan Endemic Nephropathy, has been shown (Wooding et al., 2012). To test if bitter taste receptors are also localized to the primary cilia membrane, we stained cultured kidney cells with antibodies against bitter taste receptors T2R4 and T2R43 together with the cilia marker acetylated α-tubulin. Results show that bitter taste receptors localize to the membrane of kidney primary cilia (supplementary material Fig. S9A–C). The taste receptors are functional as evidenced by treatment with the bitter compound Denatonium to elicit a Ca^{2+} response (supplementary material Fig. S9I). Of note, loss of Bbs7 did not affect cilia localization of these receptors (supplementary material Fig. S9D–F), nor affect Ca^{2+} mobilization when stimulated with the bitter compound Denatonium (supplementary material Fig. S9J), indicating that BBS7 and the BBSome is not required for ciliary membrane localization or function of bitter taste receptors.

Mutation of several ciliary membrane proteins including polycystin-1, polycystin-2, and Mecklin (MKS3), cause human diseases with phenotypes that overlap those of BBS. Therefore, we investigated the localization of both polycystin-1 and polycystin-2 in cultured *Bbs7*$^{-/-}$ primary kidney cells using antibodies against polycystin-1 and polycystin-2. BBS7 is not required for ciliary localization of polycystin-1 and polycystin-2 (Fig. 5). The fact that *Bbs7*$^{-/-}$ mice do not develop renal cysts indicates that polycystin-1 and polycystin-2 still remain functional, although we cannot rule out the possibility of subtle functional defects in the absence of BBS7.

Absence of BBS7 leads to abnormal accumulation of the dopamine D1 receptor to the ciliary membrane

Genetic studies in model organisms have shown that loss of BBS proteins lead to retrograde melanosome transport delay in zebrafish, IFT turnaround defects at the ciliary tip in *C. elegans*, accumulation of signaling proteins inside flagella in *Chlamydomonas*, and accumulation of the Smoothened inside cilia in mice (Lechtreck et al., 2009; Wei et al., 2012; Yen et al., 2006; Zhang et al., 2012a). Therefore, we investigated endogenous receptors that may accumulate inside cilia in

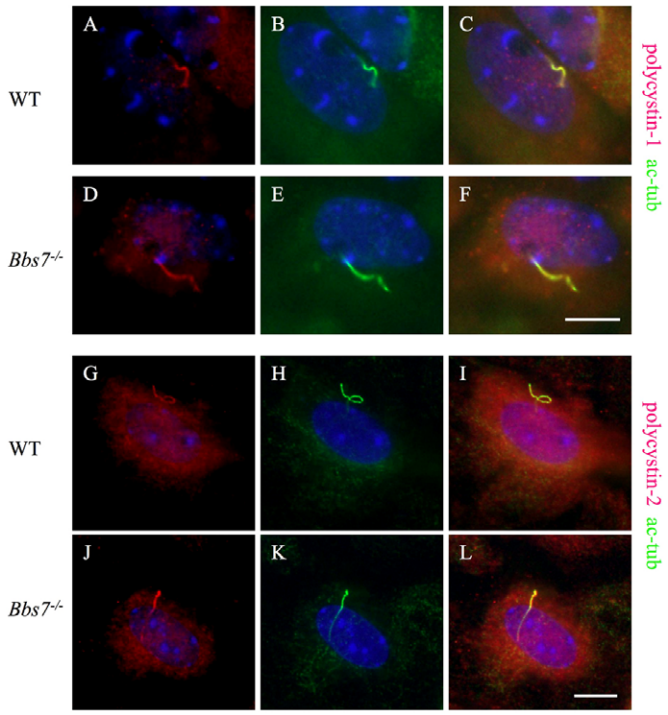

Fig. 5. BBS7 is not required for ciliary localization of polycystin-1 and polycystin-2. (**A–L**) Shown are cultured kidney cells from wild-type (A–C,G–I) and *Bbs7*$^{-/-}$ (D–F,J–L) mice stained with anti-acetylated α-tubulin (green) as a cilia marker and anti-polycystin-1 (A–F; red) and anti-polycystin-2 (G–L; red) antibody. Scale bars: 10 μm.

Bbs7$^{-/-}$ mice. The dopamine D1 receptor (D1R) has been shown to accumulate in cilia in *Bbs2*$^{-/-}$ and *Bbs4*$^{-/-}$ mice (Domire et al., 2011). To determine whether D1R accumulates in the cilia in *Bbs7*$^{-/-}$ mice, we stained brain sections from wild-type and *Bbs7*$^{-/-}$ mice with neuronal cilia marker ACIII and antibody against D1R. We cannot find any ciliary staining of D1R in wild-type brain (Fig. 6A–C). In contrast, we found multiple regions including the striatum and amygdala where D1R localizes to cilia

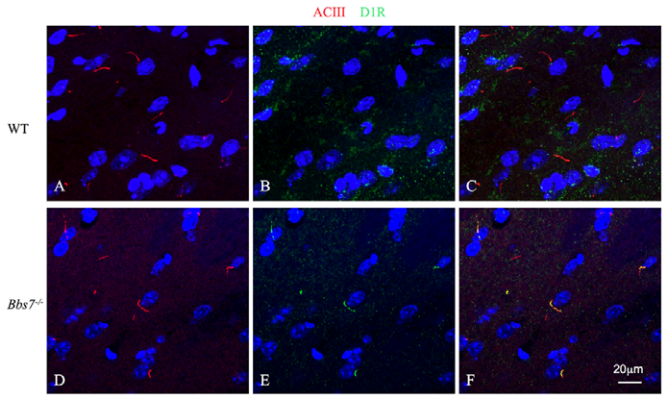

Fig. 6. Loss of BBS7 leads to abnormal accumulation of the dopamine D1 receptor inside cilia. (**A–F**) Brain sections from wild-type (A–C) and *Bbs7*$^{-/-}$ (D–F) mice were stained with anti-ACIII antibody (red) as a neuronal cilia marker and anti-D1R antibody (green). D1R accumulates inside cilia in *Bbs7*$^{-/-}$ mouse brain compared to wild-type control. Scale bar: 20 μm.

in *Bbs7*$^{-/-}$ brain (Fig. 6D–F). These data suggest that the BBSome may regulate the retrograde transport of D1R inside neuronal cilia and loss of BBS7 leads to the abnormal accumulation of the D1R to the ciliary membrane.

Discussion

The cilium is an important organelle that plays multiple roles during development and in the homeostasis of adult tissues. Motile cilia are important for such functions as clearing mucus from the lung and for the circulation of cerebral spinal fluid through the cerebral ventricles, while primary cilia are important for chemo- and mechano-sensation, as well as hedgehog and Wnt signal transduction. The importance of cilia is highlighted by findings that cilia malfunction contributes to a wide range of human diseases known as ciliopathies that include Bardet-Biedl syndrome.

BBS is a pleiotropic disorder involving many organ systems. Some BBS phenotypes such as obesity, retinal degeneration, diabetes, and hypertension have high prevalences in the general population. Therefore, the study of BBS provides a unique opportunity to uncover some of the pathways underlying or influencing these common diseases. BBS knockout mice mimic the human phenotype, thus providing a useful tool to discover the molecular mechanisms underlying the disease as well as to test novel therapies.

Although BBS mutant mice share common BBS phenotypes, phenotypic differences are observed among different BBS gene mutations. Importantly, BBS patients display phenotypic variation between and within families (Carmi et al., 1995). Physiological differences among BBS patients caused by mutations in distinct genes have been documented (Feuillan et al., 2011), suggesting that although sharing common BBS phenotypes, different BBS genes may have unique functions. BBS7 is an integral part of the BBSome and physically interacts with the BBS chaperonin complex, a finding unique to BBS7 among BBSome proteins. Absence of BBS7 affects the protein stability of BBS2 and prevents formation of the intact BBSome. However, primary cilia are still formed in the absence of BBS7. Unlike IFT gene knockouts, in which cilia do not form and lead to embryonic lethality in mice, *Bbs7*$^{-/-}$ mice can survive to adulthood and primary cilia still form in tissues including kidney, islets of the pancreas, pancreatic duct, in cultured renal epithelial cells and fibroblasts. In contrast to primary cilia, the motile cilia of ependymal cells lining cerebral ventricles and sperm flagella have severe defects in *Bbs7*$^{-/-}$ mice. The defective motile cilia are not due to the ventriculomegaly developed in the absence of BBS7 since defective motile cilia develop as early as 3 weeks in the brain ependyma. Neither do the defective motile cilia appear to be the primary cause of the ventriculomegaly. The abnormal development of neural progenitor cells may underlie the development of ventriculomegaly in this mouse model as demonstrated for other BBS mouse models since both BBS7 and BBS1 are essential for the integrity of the BBSome (Carter et al., 2012). Absence of BBS7 does not affect formation of IFT complexes, although we do not know if the motility of IFT particles is affected by absence of the BBSome. BBS genes and IFT genes appear to affect different aspects of ciliary function. Our results in mice are consistent with results from *Chlamydomonas*, highlighting the interplay between the BBSome and the IFT complex (Lechtreck et al., 2009).

We demonstrated that BBS7 protein harboring point mutations found in BBS7 patients (T211I and H323R) has a decreased ability to form the BBSome compared to normal BBS7 protein. The methods used here may provide an efficient cell-based assay system to evaluate the nature of human BBS missense mutations *in vitro*.

Recently studies have shown that cilia-related genes, such as AHI1 and FUZZY, are involved in general membrane protein trafficking rather than solely for ciliary membrane protein trafficking (Gray et al., 2009; Hsiao et al., 2009). In contrast, absence of BBS7 does not affect either clathrin independent and or clathrin dependent endocytosis pathways. Similarly, absence or mutation of BBS proteins do not affect the general secretory pathway of membrane proteins including SST3R and transferrin receptor to the plasma membrane (Jin et al., 2010) (data not shown). Although general vesicle trafficking does not seem to require BBS7 or the BBSome, trafficking of specific proteins to or from the plasma membrane may be compromised in the absence of the BBSome. One example is trafficking of the leptin receptor, which has been shown to directly interact with the BBSome (Seo et al., 2009). Interestingly, in *C. elegans*, loss of *bbs* genes leads to increased release of dense-core vesicles and enhanced activities of insulin, neuropeptide, and biogenic amine signaling pathways (Lee et al., 2011). We conclude that BBS7 and hence the BBSome are not involved in general ciliary membrane protein trafficking but rather in specific ciliary membrane protein trafficking. This conclusion is based on the observation that ciliary membrane proteins such as polycystin-1, polycystin-2, and bitter taste receptors are still localized to ciliary membrane in the total absence of BBS7 protein, which is required for BBSome assembly. In addition, evidence indicates that polycystin-1, polycystin-2, and bitter taste receptors are still functional in the absence of BBS7. In contrast, absence of BBS7 leads to the accumulation of Smo within cilia without the stimulation of Smo ligand (Zhang et al., 2012a). Other ciliary membrane proteins including SST3R and MCHR1 have been shown to localize to neuronal cilia under normal conditions, but not in the absence of BBS2 or BBS4 (Berbari et al., 2008a; Berbari et al., 2008b). However, the absence of BBS7 does not affect ciliary localization of either SST3R or MCHR1 in brain neurons or in cultured cells from $Bbs7^{-/-}$ mice (data not shown). In contrast, D1R is accumulated inside cilia in the absence of BBS7, similar to findings in $Bbs2^{-/-}$ and $Bbs4^{-/-}$ mice (Domire et al., 2011). The accumulation of D1R inside cilia may due to altered retrograde transport of D1R inside cilia in the absence of BBS7. In support of this possibility, genetic studies in zebrafish showed retrograde melanosome transport delay when the expression of *bbs* genes are suppressed (Yen et al., 2006). Furthermore, Smo accumulates inside cilia without ligand stimulation in the absence of the BBSome (Zhang et al., 2012a). The retrograde transport delay could result from altered motor activity, malfunction of the IFT complex, altered cilia axonemal structure, or specific alteration in the ability of some cargos to exit the cilium. Studies in *C. elegans* suggest that BBS proteins serve as linkers between IFT complex B and IFT complex A (Blacque et al., 2004). Loss of BBS proteins will lead to improper function of IFT complexes. In support of this possibility, double mutants of *Bbs7* and *Tg737orpk* completely lack cilia, resembling IFT complex B true knockouts (Zhang et al., 2012a). Alternatively, the primary cilia of Bbs7 mutants may also have a subtle defective in axonemal structure that may contribute to the accumulation of D1R inside cilia. The functional relevance of D1R accumulation inside cilia is currently unknown. It has been shown that BBS patients and BBS knockout mice have increased anxiety and depression (Barnett et al., 2002; Eichers et al., 2006). Interestingly, blockage of D1R signaling with pharmaceuticals attenuated conditioned freezing (a test of conditioned fear) during the retention testing (Guarraci et al., 1999a; Guarraci et al., 1999b). The localization of D1R in the striatum and amygdala regions suggests that dopamine signaling may play a role for the behavior defects observed in BBS mouse models and BBS patients.

Materials and Methods

Reagents and antibodies

Rabbit polyclonal antibody against mouse BBS2 peptide DKTARYWRIK and rabbit polyclonal antibody against mouse BBS7 peptide VLQERENYQQ were obtained from Open Biosystems (Huntsville, AL). These antibodies were affinity purified and verified in knockout mice. Monoclonal anti-β-tubulin, polyclonal anti-β-actin, monoclonal anti-acetylated tubulin, monoclonal anti-γ-tubulin, rabbit polyclonal anti-BBS8 and BBS9 were purchased from Sigma (St. Louis, MO). Goat anti-BBS1 (N-20), goat anti-BBS2 (C-16) antibodies, and mouse anti-D1R antibody were purchased from Santa Cruz Biotechnology (Santa Cruz Biotechnology, CA). Anti-T2R4 rabbit polyclonal antibody and rabbit anti-T2R43 rabbit polyclonal antibody were purchased from Thermo Scientific (Pittsburgh, PA). Alexa 488 conjugated cholera toxin and Alexa 568 conjugated human transferring receptor were purchased from Invitrogen (Carlsbad, CA). Rabbit polyclonal anti-polycystin-1 was a gift from Dr Oxana Ibraghimov-Beskrovnaya (Genzyme Corporation). Rabbit polyclonal anti-polycystin-2 antibody was a gift from Dr Stefan Somlo (Yale University) and Dr Gregory Pazour (University of Massachusetts Medical School).

Generation of *Bbs7* knockout mice

PCR was used to amplify 5′ and 3′ regions of the *Bbs7* gene from 129/SvJ genomic DNA and cloned into the targeting vector pOSDUPDEL (a gift from O. Smithies, University of North Carolina, Chapel Hill, NC). The vector was linearized and electroporated into R1 embryonic stem (ES) cells (129×1/SvJ3 129S1/Sv). G418 and ganciclovir-resistant clones were screened by long range PCR to identify correctly targeted ES cell lines. Two independent ES cell lines were used to produce chimeras. Chimeric animals were used to generate *Bbs7* heterozygous mice on a mixed genetic background by mating with C57BL/6J mice. Heterozygous mice were intercrossed, and the progeny were genotyped by PCR. All studies adhered to the guidelines established for the care and use of experimental animals and were approved by the Animal Care and Use Committee of the University of Iowa.

RNA isolation and RT-PCR analysis

RNA was isolated from 2.5-month-old wild-type and $Bbs7^{-/-}$ mouse testes using TRIzol reagent (Invitrogen, Carlsbad, CA). cDNA was prepared from 1 µg total RNA using SuperScript III reverse transcriptase (Invitrogen, Carlsbad, CA).

Western blot analysis

Wild-type and *Bbs7* mutant testes were disrupted by TISSUEMISER (Fisher Scientific, Pittsburgh, PA) in lysis buffer (1× PBS, 1% Triton X-100 and protease inhibitor from Roche, Indianapolis, IN). The disrupted tissues were frozen in liquid nitrogen and thawed in a room temperature water bath. This freeze-thaw cycle was repeated three times. The lysates were then centrifuged at 20,000×***g*** for 15 minutes and the concentration of the supernatants was measured using the Bio-Rad Dc protein assay (Hercules, CA).

Proteins were separated by electrophoresis using 4–12% NuPAGE Bis-Tris gels (Invitrogen, Carlsbad, CA) followed by transfer to nitrocellulose membranes and were detected by SuperSignal Dura extended substrate (Pierce, Rockford, IL).

Histological analysis of $Bbs7^{-/-}$ mice

Hematoxylin & eosin staining of eyes and testes from 4–8-month-old *Bbs7* mutant and age-matched controls was carried out as described. Coronal brain sections of 60–100 µm from 4–8-month-old $Bbs7^{-/-}$ animals and age-matched controls were stained with Neutral Red and photographed with an Olympus SZX12 stereomicroscope as described (Davis et al., 2007).

Weight studies

Food intake of individually caged $Bbs7^{-/-}$ animals was compared with $Bbs7^{+/-}$ and wild-type control animals ranging in age from 4 to 28 weeks using an average of six animals per group. Weight was recorded weekly beginning at weaning.

Transmission electron microscopy

Mice were perfused with half-strength Karnovsky's fixative and tissues were dissected and fixed in half-strength Karnovsky's fixative for several hours prior to osmium post-fixation, dehydration, and embedding in Epon 812. Transmission electron micrographs were taken as described previously (Swiderski et al., 2007).

Generation of human BBS2 and BBS7 mutant deletion constructs and point mutations

BBS7 deletion mutants were generated by PCR and cloned into mammalian expression vectors pCS2+. All deletion mutants were verified by direct sequencing. BBS7 point mutations were generated by site-directed mutagenesis (Stratagene, La Jolla, CA) using N-terminal FLAG-tagged wild-type BBS7 as template and verified by sequencing.

Immunoprecipitation

Differentially tagged human BBS genes were co-transfected into 293T cells. Forty-eight hours after transfection, the cells were lysed in lysis buffer (1× PBS, 1% Triton X-100, and protease inhibitor, Roche, Indianapolis, IN) and spun at 20,000×***g*** for 15 minutes at 4℃. The supernatants were cleared by incubation with protein G beads (Pierce, Rockford, IL). Cleared lysates were incubated with antibodies against corresponding tags for 4 hours. Protein G beads were then added and incubated for another 4 hours. The beads were washed four times with lysis buffer and the interactions were detected by western blotting.

Immunofluorescence microscopy

Cells were fixed in 4% paraformaldhyde in PBS or fixed with cold methanol for 5 minutes (for γ-tubulin stain) and permeabilized with 0.2% Triton X-100 in room temperature for 7 minutes. Cells were washed 3× PBS and blocked with blocking buffer (1% BSA in PBS). Primary antibodies were diluted in blocking buffer and incubated at room temperature for 1 hour. Cells were washed 3× PBS, blocked with blocking buffer, then incubated with Alexa Fluor 488 or Alexa Fluor 568 labeled secondary antibodies (Invitrogen, Carlsbad, CA). Nuclei were stained with DAPI (Sigma, St. Louis, MO).

Kidney primary cell culture

Kidneys from wild-type and *Bbs7*$^{-/-}$ mice were dissected and sterilized by placement into 100% ethanol for 5 seconds, then minced with scissors. The tissues were washed once with cold DMEM/F-12 without serum. 20 ml of pronase (1 mg/ml; Roche, Indianapolis, IN) was added to the tissues and kept at room temperature for one hour. The tissues were then washed once with cold DMEM/F-12 and incubated with 20 ml 1× Trypsin-EDTA at room temperature for 2 hours. Tissues were pelleted at 500 ***g*** for 5 minutes and re-suspended in 30 ml DMEM/F-12 with 10% serum. The re-suspended tissues were plated in three 10-cm dishes coated with poly-L-lysine (Sigma, St. Louis, MO).

Cholera toxin and transferrin receptor endocytosis

Cholera toxin and transferrin receptor endocytosis assays were performed as described by Hsiao et al. (Hsiao et al. 2009).

Calcium imaging

Calcium imaging was performed as previously described (Shah et al., 2009). Cultured kidney cells from wild-type and *Bbs7*$^{-/-}$ mice were loaded with 1 μM Fura2 am, calcium concentration changes in epithelia were assessed using an inverted microscope (Nikon Eclipse TE200, Nikon Instruments Inc., Melville, NY), and the data were analyzed using NIS-Elements software (Nikon). Denatonium was applied apically at the indicated concentrations. PBS was used as control.

Author contributions

Q.Z., E.M.S. and V.C.S. designed the experiments, interpreted the data and wrote the manuscript. Q.Z., D.N., T.V., J.S., R.S., T.Y., C.S., C.S.C., G.K. and K.B. performed the experiments.

Funding

This work is supported by the National Institutes of Health [grant numbers EY110298, EY01768 to V.C.S.]. V.C.S. and E.M.S. are Investigators of the Howard Hughes Medical Institute. Deposited in PMC for release after 6 months.

Supplementary material available online at
http://jcs.biologists.org/lookup/suppl/doi:10.1242/jcs.111740/-/DC1

References

Barnett, S., Reilly, S., Carr, L., Ojo, I., Beales, P. L. and Charman, T. (2002). Behavioural phenotype of Bardet-Biedl syndrome. *J. Med. Genet.* **39**, e76.

Berbari, N. F., Johnson, A. D., Lewis, J. S., Askwith, C. C. and Mykytyn, K. (2008a). Identification of ciliary localization sequences within the third intracellular loop of G protein-coupled receptors. *Mol. Biol. Cell* **19**, 1540-1547.

Berbari, N. F., Lewis, J. S., Bishop, G. A., Askwith, C. C. and Mykytyn, K. (2008b). Bardet-Biedl syndrome proteins are required for the localization of G protein-coupled receptors to primary cilia. *Proc. Natl. Acad. Sci. USA* **105**, 4242-4246.

Blacque, O. E., Reardon, M. J., Li, C., McCarthy, J., Mahjoub, M. R., Ansley, S. J., Badano, J. L., Mah, A. K., Beales, P. L., Davidson, W. S. et al. (2004). Loss of C. elegans BBS-7 and BBS-8 protein function results in cilia defects and compromised intraflagellar transport. *Genes Dev.* **18**, 1630-1642.

Carmi, R., Elbedour, K., Stone, E. M. and Sheffield, V. C. (1995). Phenotypic differences among patients with Bardet-Biedl syndrome linked to three different chromosome loci. *Am. J. Med. Genet.* **59**, 199-203.

Carter, C. S., Vogel, T. W., Zhang, Q., Seo, S., Swiderski, R. E., Moninger, T. O., Cassell, M. D., Thedens, D. R., Keppler-Noreuil, K. M., Nopoulos, P. et al. (2012). Abnormal development of NG2+PDGFR-α+ neural progenitor cells leads to neonatal hydrocephalus in a ciliopathy mouse model. *Nat. Med.* **18**, 1797-1804.

Davis, R. E., Swiderski, R. E., Rahmouni, K., Nishimura, D. Y., Mullins, R. F., Agassandian, K., Philp, A. R., Searby, C. C., Andrews, M. P., Thompson, S. et al. (2007). A knockin mouse model of the Bardet-Biedl syndrome 1 M390R mutation has cilia defects, ventriculomegaly, retinopathy, and obesity. *Proc. Natl. Acad. Sci. USA* **104**, 19422-19427.

Domire, J. S., Green, J. A., Lee, K. G., Johnson, A. D., Askwith, C. C. and Mykytyn, K. (2011). Dopamine receptor 1 localizes to neuronal cilia in a dynamic process that requires the Bardet-Biedl syndrome proteins. *Cell. Mol. Life Sci.* **68**, 2951-2960.

Eichers, E. R., Abd-El-Barr, M. M., Paylor, R., Lewis, R. A., Bi, W., Lin, X., Meehan, T. P., Stockton, D. W., Wu, S. M., Lindsay, E. et al. (2006). Phenotypic characterization of Bbs4 null mice reveals age-dependent penetrance and variable expressivity. *Hum. Genet.* **120**, 211-226.

Fath, M. A., Mullins, R. F., Searby, C., Nishimura, D. Y., Wei, J., Rahmouni, K., Davis, R. E., Tayeh, M. K., Andrews, M., Yang, B. et al. (2005). Mkks-null mice have a phenotype resembling Bardet-Biedl syndrome. *Hum. Mol. Genet.* **14**, 1109-1118.

Feuillan, P. P., Ng, D., Han, J. C., Sapp, J. C., Wetsch, K., Spaulding, E., Zheng, Y. C., Caruso, R. C., Brooks, B. P., Johnston, J. J. et al. (2011). Patients with Bardet-Biedl syndrome have hyperleptinemia suggestive of leptin resistance. *J. Clin. Endocrinol. Metab.* **96**, E528-E535.

Gray, R. S., Abitua, P. B., Wlodarczyk, B. J., Szabo-Rogers, H. L., Blanchard, O., Lee, I., Weiss, G. S., Liu, K. J., Marcotte, E. M., Wallingford, J. B. et al. (2009). The planar cell polarity effector Fuz is essential for targeted membrane trafficking, ciliogenesis and mouse embryonic development. *Nat. Cell Biol.* **11**, 1225-1232.

Guarraci, F. A., Frohardt, R. J. and Kapp, B. S. (1999a). Amygdaloid D1 dopamine receptor involvement in Pavlovian fear conditioning. *Brain Res.* **827**, 28-40.

Guarraci, F. A., Frohardt, R. J., Young, S. L. and Kapp, B. S. (1999b). A functional role for dopamine transmission in the amygdala during conditioned fear. *Ann. N. Y. Acad. Sci.* **877**, 732-736.

Hsiao, Y. C., Tong, Z. J., Westfall, J. E., Ault, J. G., Page-McCaw, P. S. and Ferland, R. J. (2009). Ahi1, whose human ortholog is mutated in Joubert syndrome, is required for Rab8a localization, ciliogenesis and vesicle trafficking. *Hum. Mol. Genet.* **18**, 3926-3941.

Jin, H., White, S. R., Shida, T., Schulz, S., Aguiar, M., Gygi, S. P., Bazan, J. F. and Nachury, M. V. (2010). The conserved Bardet-Biedl syndrome proteins assemble a coat that traffics membrane proteins to cilia. *Cell* **141**, 1208-1219.

Kulaga, H. M., Leitch, C. C., Eichers, E. R., Badano, J. L., Lesemann, A., Hoskins, B. E., Lupski, J. R., Beales, P. L., Reed, R. R. and Katsanis, N. (2004). Loss of BBS proteins causes anosmia in humans and defects in olfactory cilia structure and function in the mouse. *Nat. Genet.* **36**, 994-998.

Lechtreck, K. F., Johnson, E. C., Sakai, T., Cochran, D., Ballif, B. A., Rush, J., Pazour, G. J., Ikebe, M. and Witman, G. B. (2009). The Chlamydomonas reinhardtii BBSome is an IFT cargo required for export of specific signaling proteins from flagella. *J. Cell Biol.* **187**, 1117-1132.

Lee, B. H., Liu, J., Wong, D., Srinivasan, S. and Ashrafi, K. (2011). Hyperactive neuroendocrine secretion causes size, feeding, and metabolic defects of C. elegans Bardet-Biedl syndrome mutants. *PLoS Biol.* **9**, e1001219.

Lee, R. J., Xiong, G., Kofonow, J. M., Chen, B., Lysenko, A., Jiang, P., Abraham, V., Doghramji, L., Adappa, N. D., Palmer, J. N. et al. (2012). T2R38 taste receptor polymorphisms underlie susceptibility to upper respiratory infection. *J. Clin. Invest.* **122**, 4145-4159.

Mykytyn, K., Mullins, R. F., Andrews, M., Chiang, A. P., Swiderski, R. E., Yang, B., Braun, T., Casavant, T., Stone, E. M. and Sheffield, V. C. (2004). Bardet-Biedl syndrome type 4 (BBS4)-null mice implicate Bbs4 in flagella formation but not global cilia assembly. *Proc. Natl. Acad. Sci. USA* **101**, 8664-8669.

Nachury, M. V., Loktev, A. V., Zhang, Q., Westlake, C. J., Peränen, J., Merdes, A., Slusarski, D. C., Scheller, R. H., Bazan, J. F., Sheffield, V. C. et al. (2007). A core complex of BBS proteins cooperates with the GTPase Rab8 to promote ciliary membrane biogenesis. *Cell* **129**, 1201-1213.

Nishimura, D. Y., Fath, M., Mullins, R. F., Searby, C., Andrews, M., Davis, R., Andorf, J. L., Mykytyn, K., Swiderski, R. E., Yang, B. et al. (2004). Bbs2-null mice have neurosensory deficits, a defect in social dominance, and retinopathy associated with mislocalization of rhodopsin. *Proc. Natl. Acad. Sci. USA* **101**, 16588-16593.

Rahmouni, K., Fath, M. A., Seo, S., Thedens, D. R., Berry, C. J., Weiss, R., Nishimura, D. Y. and Sheffield, V. C. (2008). Leptin resistance contributes to

obesity and hypertension in mouse models of Bardet-Biedl syndrome. *J. Clin. Invest.* **118**, 1458-1467.

Sattar, S. and Gleeson, J. G. (2011). The ciliopathies in neuronal development: a clinical approach to investigation of Joubert syndrome and Joubert syndrome-related disorders. *Dev. Med. Child Neurol.* **53**, 793-798.

Seo, S., Guo, D. F., Bugge, K., Morgan, D. A., Rahmouni, K. and Sheffield, V. C. (2009). Requirement of Bardet-Biedl syndrome proteins for leptin receptor signaling. *Hum. Mol. Genet.* **18**, 1323-1331.

Seo, S., Baye, L. M., Schulz, N. P., Beck, J. S., Zhang, Q., Slusarski, D. C. and Sheffield, V. C. (2010). BBS6, BBS10, and BBS12 form a complex with CCT/TRiC family chaperonins and mediate BBSome assembly. *Proc. Natl. Acad. Sci. USA* **107**, 1488-1493.

Shah, A. S., Ben-Shahar, Y., Moninger, T. O., Kline, J. N. and Welsh, M. J. (2009). Motile cilia of human airway epithelia are chemosensory. *Science* **325**, 1131-1134.

Swiderski, R. E., Nishimura, D. Y., Mullins, R. F., Olvera, M. A., Ross, J. L., Huang, J., Stone, E. M. and Sheffield, V. C. (2007). Gene expression analysis of photoreceptor cell loss in bbs4-knockout mice reveals an early stress gene response and photoreceptor cell damage. *Invest. Ophthalmol. Vis. Sci.* **48**, 3329-3340.

Wei, Q., Zhang, Y., Li, Y., Zhang, Q., Ling, K. and Hu, J. (2012). The BBSome controls IFT assembly and turnaround in cilia. *Nat. Cell Biol.* **14**, 950-957.

Wooding, S. P., Atanasova, S., Gunn, H. C., Staneva, R., Dimova, I. and Toncheva, D. (2012). Association of a bitter taste receptor mutation with Balkan Endemic Nephropathy (BEN). *BMC Med. Genet.* **13**, 96.

Yen, H. J., Tayeh, M. K., Mullins, R. F., Stone, E. M., Sheffield, V. C. and Slusarski, D. C. (2006). Bardet-Biedl syndrome genes are important in retrograde intracellular trafficking and Kupffer's vesicle cilia function. *Hum. Mol. Genet.* **15**, 667-677.

Zhang, Q., Nishimura, D., Seo, S., Vogel, T., Morgan, D. A., Searby, C., Bugge, K., Stone, E. M., Rahmouni, K. and Sheffield, V. C. (2011). Bardet-Biedl syndrome 3 (Bbs3) knockout mouse model reveals common BBS-associated phenotypes and Bbs3 unique phenotypes. *Proc. Natl. Acad. Sci. USA* **108**, 20678-20683.

Zhang, Q., Seo, S., Bugge, K., Stone, E. M. and Sheffield, V. C. (2012a). BBS proteins interact genetically with the IFT pathway to influence SHH-related phenotypes. *Hum. Mol. Genet.* **21**, 1945-1953.

Zhang, Q., Yu, D., Seo, S., Stone, E. M. and Sheffield, V. C. (2012b). Intrinsic protein-protein interaction-mediated and chaperonin-assisted sequential assembly of stable bardet-biedl syndrome protein complex, the BBSome. *J. Biol. Chem.* **287**, 20625-20635.

Fig. S1. Generation of *Bbs7* knockout mice. (A) Diagram of the Bbs7 targeting vector and the resulting recombination product. (B) RT-PCR analysis of *Bbs7* expression in testis total RNA from wild type (WT) and *Bbs7*$^{-/-}$ animals. (C) Western blot analysis of wild type (WT) and *Bbs7*$^{-/-}$ testes confirms the absence of the 75 kDa BBS7 protein. Asterisk (*) corresponds to a non-specific cross-reacting protein that was used as a loading control. (D) Mating of *Bbs7*$^{+/-}$ heterozygotes resulted in a sub-Mendelian ratio of the offspring (n=387).

Fig. S2. The cerebellum of *Bbs7*$^{-/-}$ mice appears normal. Shown are H & E stains of WT (A, C) and *Bbs7*$^{-/-}$ (B, D) cerebellum. No apparent changes of overall morphology or foliation of the cerebellum. The Purkinje cells in the cerebellum also appear normal (C, D), as indicated by black arrows.

Fig. S3. Bbs7 is not required for primary ciliogenesis. Shown in A and B are immunofluorescence staining of cultured kidney cells stained with the cilia marker anti-acetylated tubulin (red) and the basal body marker anti-γ-tubulin (green). C and D are OCT kidney tissue sections stained with anti-acetylated tubulin (green). The tubule in the kidney is circled by the white dotted line. E and F are OCT pancreatic tissue sections stained with anti-acetylated tubulin (red). The islet of Langerhans is circled by the white dotted line.

Fig. S4. Normal 9+2 axonemal structures of cilia in WT and *Bbs7*$^{-/-}$ mice trachea. Shown are cross sections of TEM images of trachea cilia from WT (A) and *Bbs7* mutant mice (B).

Fig. S5. Mapping the interaction domains between BBS7 and BBS2. (A) BBS7 domain structure generated by online Pfam program and the summary of the BBS7 deletion mutants interacting with BBS2; Homozygous point mutations found in BBS patients are labeled on the top of the diagram; (B) BBS2 domain structure generated by online Pfam program and the summary of the BBS2 deletion mutants interacting with BBS7. (C) Deletion of the coil-coiled domain in BBS7 does not affect its association with endogenous BBSome subunits, while deletion of the coil-coiled domain of BBS2 disrupts its association with some of the endogenous BBSome subunits such as BBS7, but has less effect on other BBSome subunits such as BBS1 and BBS9.

Fig. S6. BBS7 is not required for IFT complex formation or ciliary localization. Shown in (A) immunoprecipitation analysis of IFT complex B formation in WT and *Bbs7*$^{-/-}$ testes lysates using antibody against IFT complex B subunit IFT57. (B) Sucrose gradient analysis of protein lysates from WT and *Bbs7*$^{-/-}$ testes tissues confirmed that the IFT complex is not affected by loss of BBS7. (C) Immunofluorescent staining of cultured kidney primary cells from WT and *Bbs7*$^{-/-}$ mice show that loss of BBS7 does not affect primary ciliogenesis and ciliary localization of IFT complex B protein, IFT88. Bar represents 10 μm.

Fig. S7. **Cholera toxin endocytosis in WT and *Bbs7*$^{-/-}$ cells.** Shown are Alexa 488 labeled cholera toxin taken up by cultured WT (A, C, E, G) and *Bbs7*$^{-/-}$ (B, D, F, H) kidney primary cells at different time points. (I) Quantitation of percentage of cells with endocytosed cholera toxin in the perinuclear region.

Fig. S8. **Transferrin receptor endocytosis in WT and *Bbs7*$^{-/-}$ cells.** Shown are Alexa 568 labeled human transferrin receptor uptake by cultured WT (A, C, E, G, I) and *Bbs7*$^{-/-}$ (B, D, F, H, J) mouse kidney primary cells at different time points. (K) Quantitation of percentage of cells with endocytosed transferrin receptor in the perinuclear region.

Fig. S9. BBS7 is not required for the ciliary localization of bitter taste receptors. Immunofluorescent staining of cultured WT (A, B, C) and *Bbs7*$^{-/-}$ (D, E, F) kidney cells are shown. Bitter taste receptors T2R4 and T2R43 can still localize to the ciliary membrane in *Bbs7*$^{-/-}$ mice kidney cells (D, E, F). The antibody staining is specific as shown by staining with anti-T2R4 and T2R43 antibody alone (G, H). (Scale bar, 10 μm). (I) Bitter taste receptors in the kidney cells are functional. Cultured kidney cells were loaded with Fura2-AM and fluorescence imaging was used to assess changes in Ca^{++} concentration when treated with the bitter compound, Denatonium, indicated as the ratio of emission when excited at 340 nm versus 380 nm ($A_{340/380}$). Ionomycin was used as a positive control. (J) Absence of BBS7 does not affect the response to the bitter compound as indicated by the ratio of emission when excited at 340 nm versus 380 nm ($A_{340/380}$).

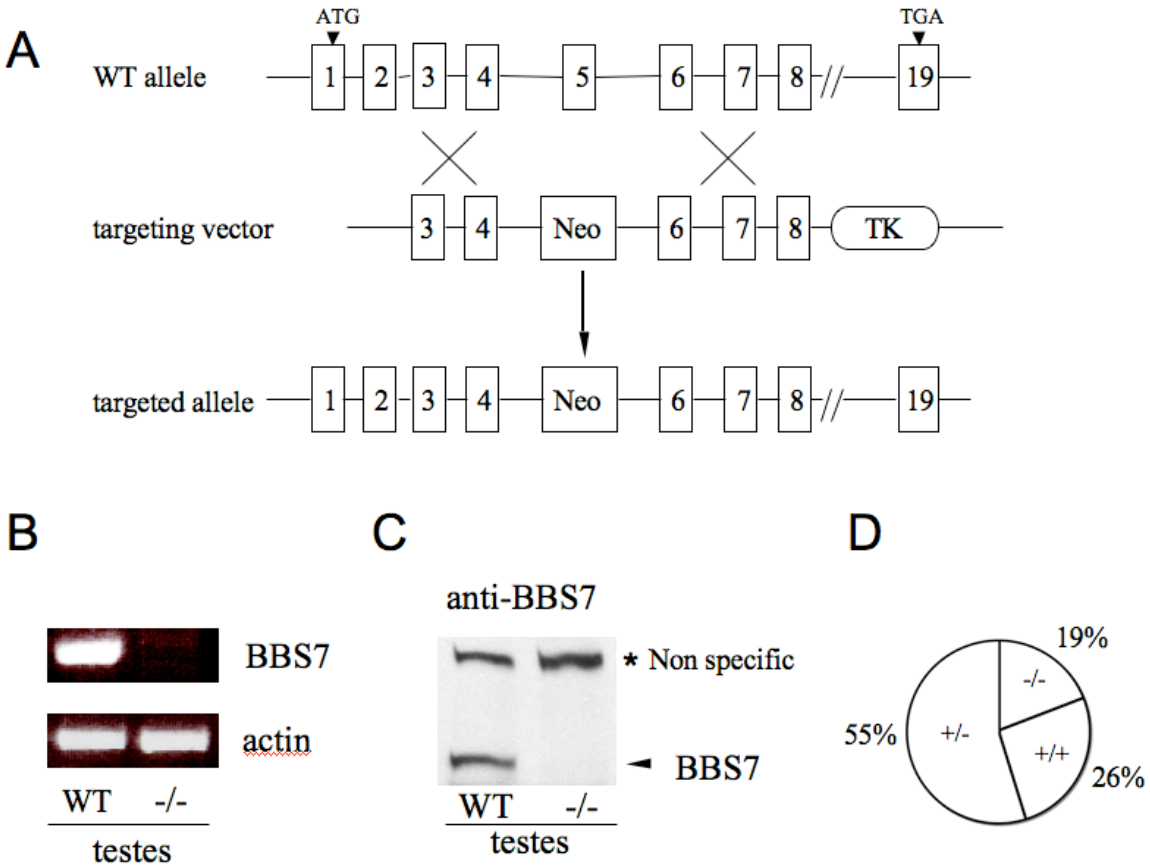
A
ATG
TGA
WT allele
1
2
3
4
5
6
7
8
19
targeting vector
3
4
Neo
6
7
8
TK
targeted allele
1
2
3
4
Neo
6
7
8
19
B
BBS7
actin
WT
-/-
testes
C
anti-BBS7
* Non specific
BBS7
WT
-/-
testes
D
19%
-/-
55%
+/-
+/+
26%

Figure S1

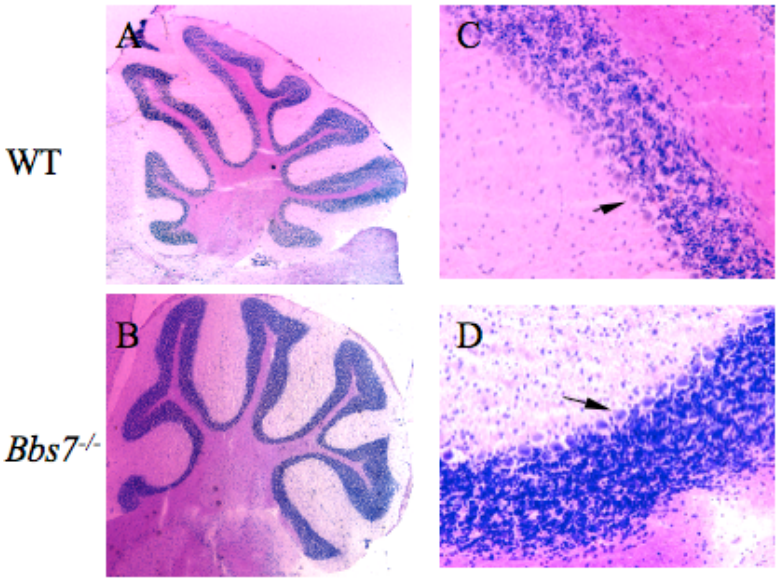

Figure S2

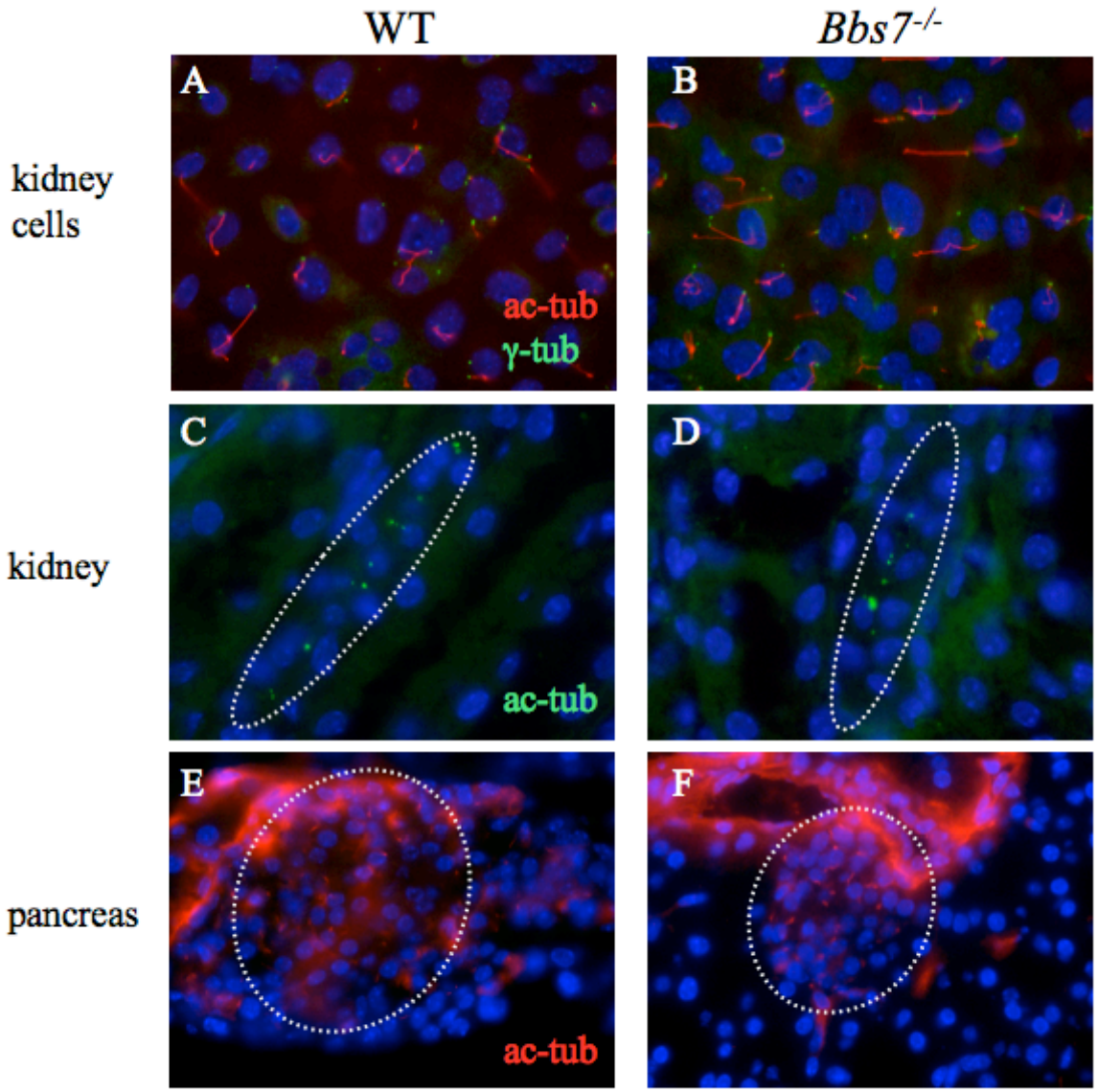
WT
Bbs7-/-
kidney cells
kidney
pancreas
A
B
C
D
E
F
ac-tub
γ-tub
ac-tub
ac-tub

Figure S3

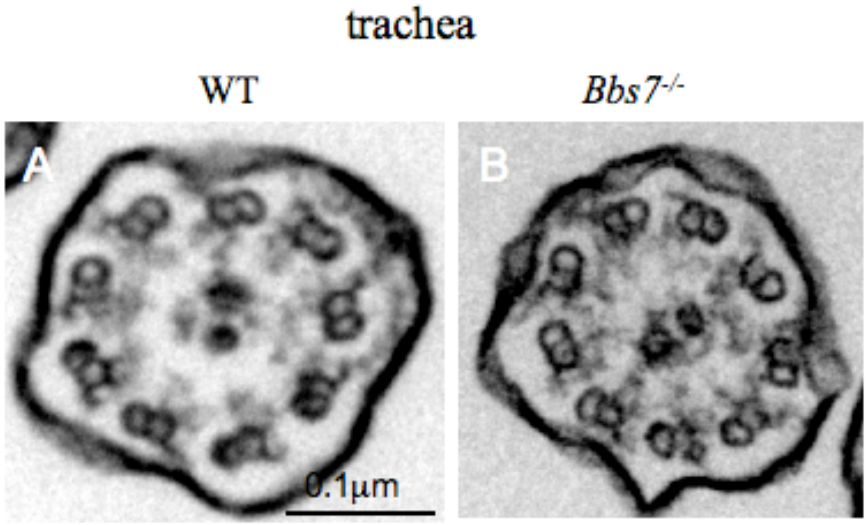

Figure S4

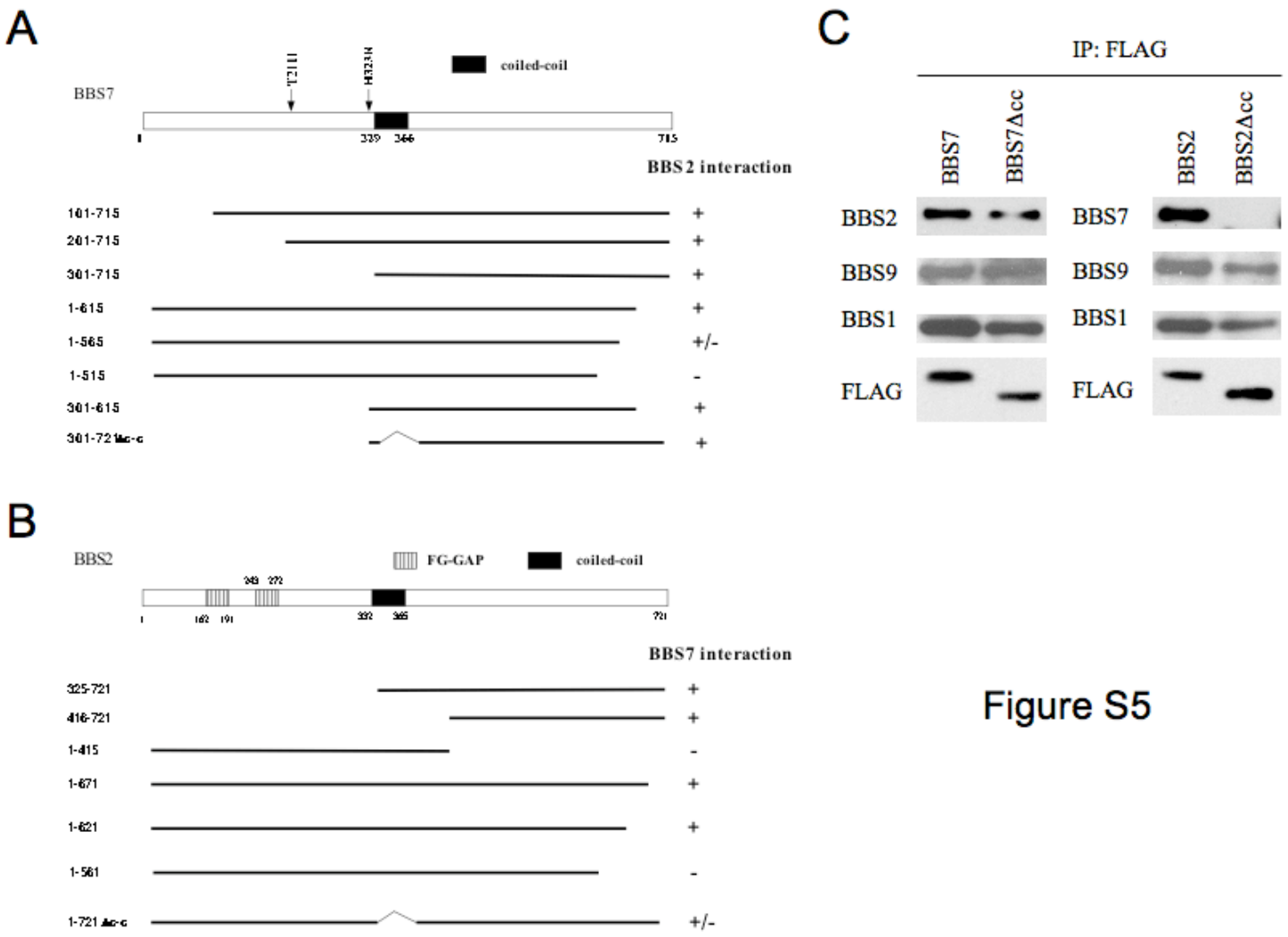
A
BBS7
coiled-coil
339 366
715
BBS2 interaction
101-715 +
201-715 +
301-715 +
1-615 +
1-565 +/-
1-515 -
301-615 +
B
BBS2
FG-GAP
coiled-coil
162 191
332 365
721
BBS7 interaction
325-721 +
416-721 +
1-415 -
1-671 +
1-621 +
1-561 -
C
IP: FLAG
BBS7
BBS7Δcc
BBS2
BBS2Δcc
BBS2
BBS9
BBS1
FLAG
BBS7
BBS9
BBS1
FLAG

Figure S5

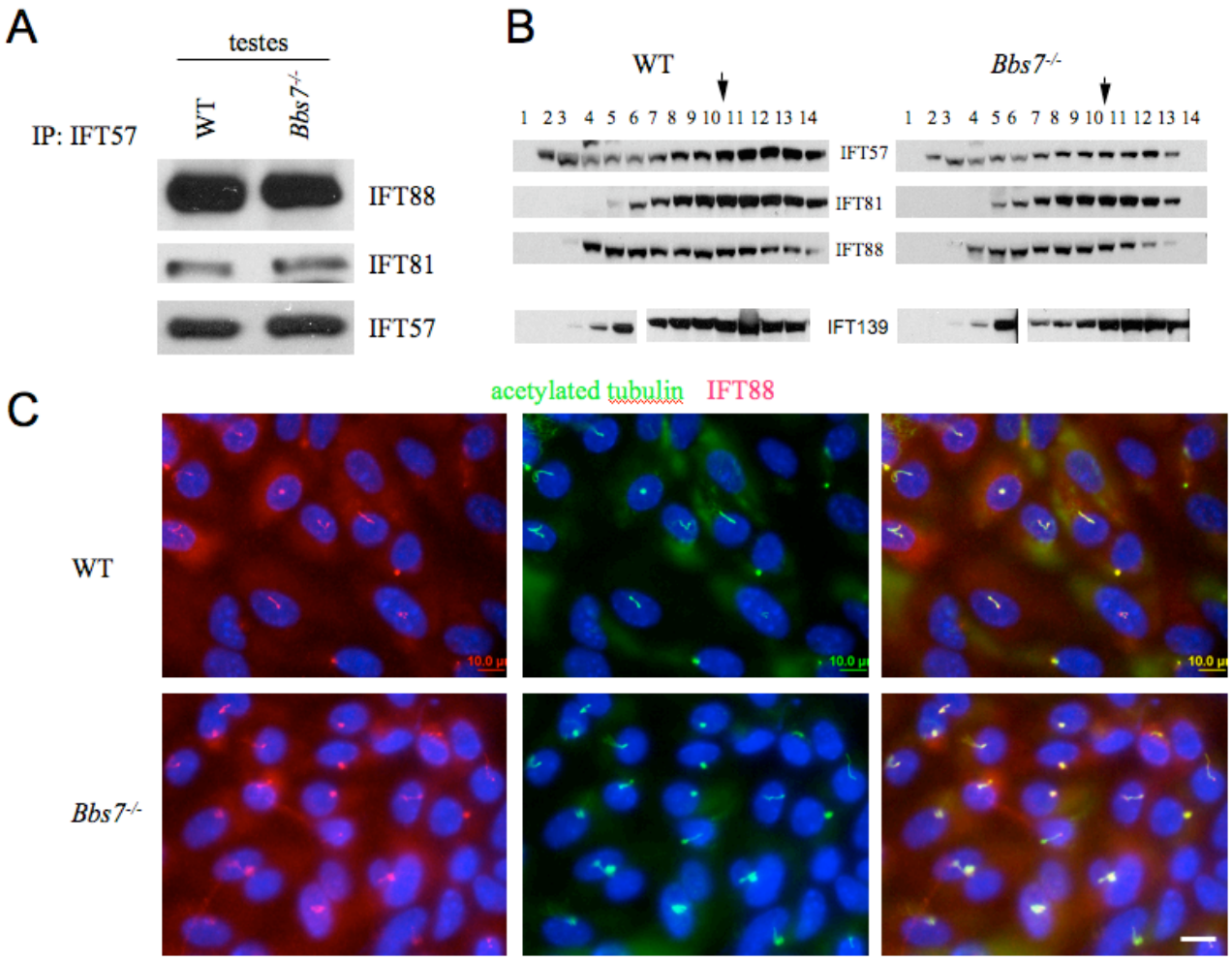
A
testes
WT
Bbs7-/-
IP: IFT57
IFT88
IFT81
IFT57
B
WT
Bbs7-/-
1 2 3 4 5 6 7 8 9 10 11 12 13 14
IFT57
IFT81
IFT88
IFT139
C
acetylated tubulin
IFT88
WT
Bbs7-/-

Figure S6

Figure S7

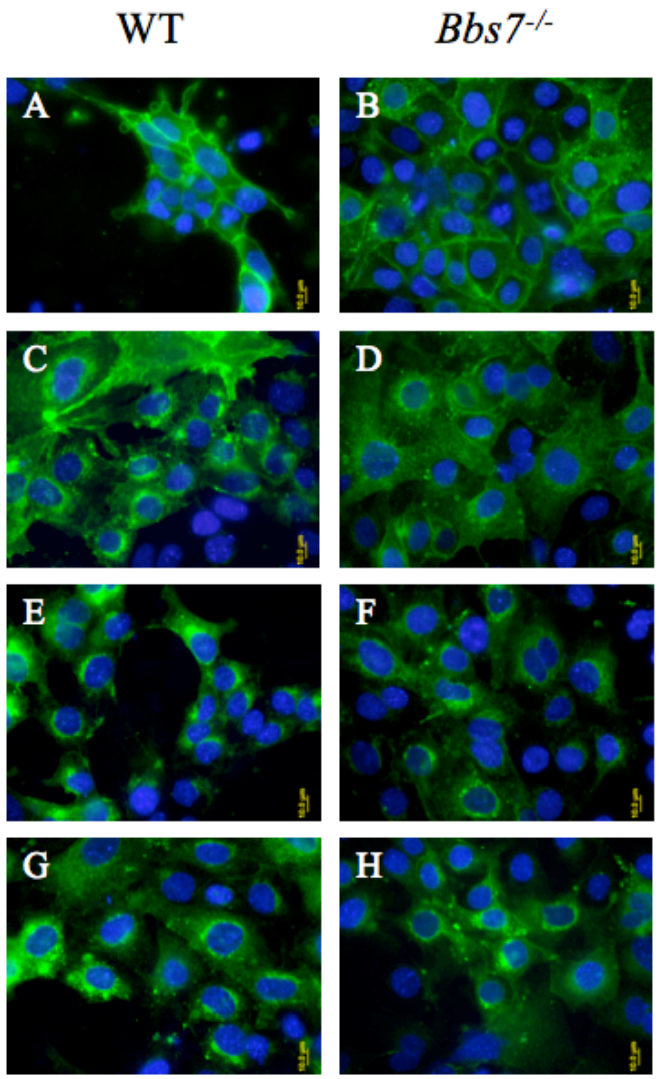

cholera toxin endocytosis

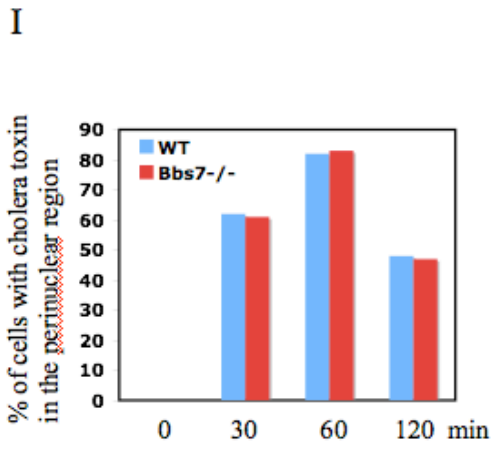

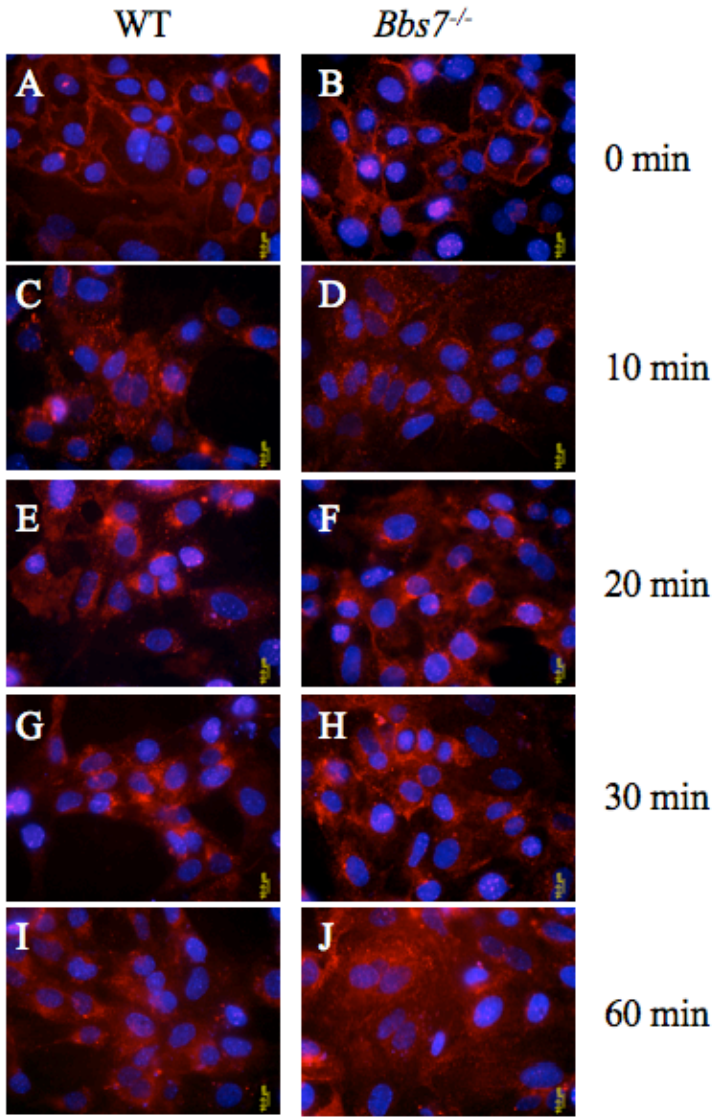

Figure S8

Transferrin receptor endocytosis

K

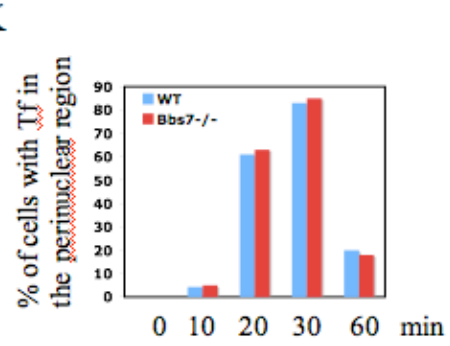

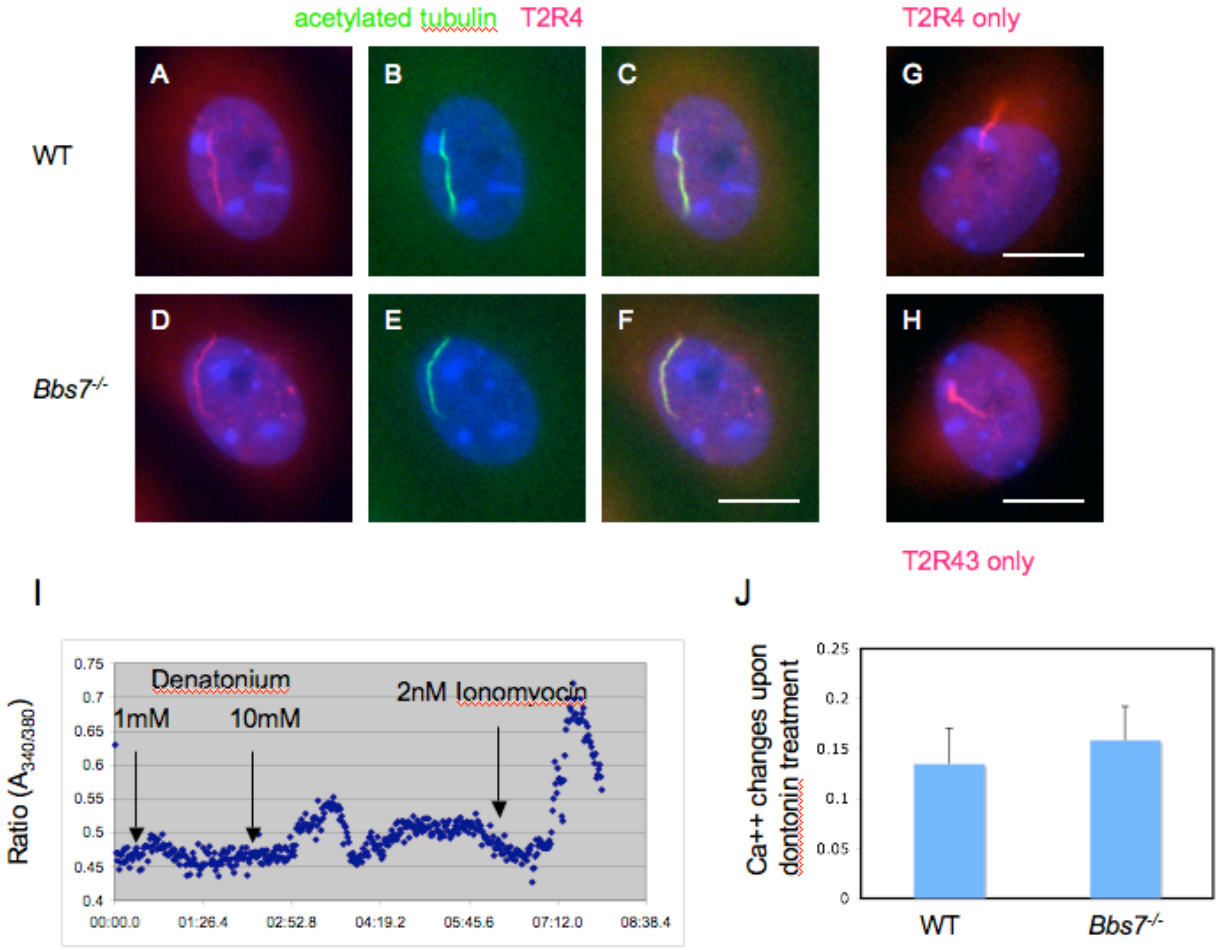
acetylated tubulin
T2R4
T2R4 only
WT
Bbs7-/-
A
B
C
G
D
E
F
H
T2R43 only
I
J
Ratio (A340/380)
Denatonium
1mM
10mM
2nM Ionomycin
0.75
0.7
0.65
0.6
0.55
0.5
0.45
0.4
00:00.0
01:26.4
02:52.8
04:19.2
05:45.6
07:12.0
08:38.4
Ca++ changes upon dontonin treatment
0.25
0.2
0.15
0.1
0.05
0
WT
Bbs7-/-

Figure S9